Effect of Wall Properties on the Behavior of Bench-Scale Reverse Flow Reactors

Miguel A. G. Hevia, Salvador Ordóñez, and Fernando V. Díez
Departamento de Ingeniería Química y Tecnología del Medio Ambiente, Universidad de Oviedo, C/ Julián Clavería 8, 33006 Oviedo, Spain

DOI 10.1002/aic.10920
Published online June 16, 2006 in Wiley InterScience (www.interscience.wiley.com).

Although in big-sized industrial fixed bed combustors the effect of the reactor wall in heat transfer phenomena can often be neglected, this is not so for smaller reactors. This article focuses on the study of the wall influence (especially the effect of the wall physical properties, such as thickness, heat capacity, and thermal conductivity) in the performance of bench scale reverse flow reactors. The reaction considered is the combustion of methane lean mixtures, very relevant for environmental applications, and useful as a model for VOC combustion. The study was carried out both experimentally (in a bench-scale apparatus, equipped with a temperature control system that minimizes the heat exchange between the reactor and the surroundings) and by simulations (using a heterogeneous one-dimensional model). The results confirm the importance of the wall effects on the performance of reverse flow reactors, and the influence of the physical properties of the wall is reported. So, higher wall thermal conductivity leads to a decrease in the reactor stability range. High wall heat capacity is also detrimental for the reactor performance, although its effect depends strongly on the range of the wall thermal conductivity considered. Finally, the stability range of reverse flow reactors is less affected by wall effects as the surface velocity increases. © 2006 American Institute of Chemical Engineers *AIChE J,* 52: 3203–3209, 2006

Keywords: reverse-flow afterburners, autothermal combustion, wall effects, thermal conductivity, heat capacity, adiabatic reactor

Introduction

Reverse-Flow catalytic Reactors (RFR) are catalytic reactors in which the feed flow direction is periodically reversed, and the reactor is then forced to run unsteadily. When an exothermic reaction is carried out in this type of reactor, the bed ends act as heat regenerators. When the time interval at which the flow is reversed is short enough, as to avoid the high temperature wave to leave the bed, the heat of reaction is trapped inside the bed during the startup. Hence, a great increase in energy efficiency is achieved, allowing auto-thermal operation even for feeds with very low adiabatic temperature increase. RFR have then the potential of decreasing to great extent, or even eliminating, the auxiliary fuel consumed in the catalytic abatement of cold and lean Volatile Organic Compounds (VOC) mixtures in air. Although the nature of the operation is intrinsically unsteady, after a certain number of cycles, the reactor reaches a state in which its characteristic variables repeat periodically. This state is called Periodic Steady State or Pseudo-Steady State (PSS).

RFR have been extensively investigated in the last 30 years. The group of Matros was the pioneer in the study of RFR, applied first to SO_2 oxidation,[1] exploring also other reactions they can be applied to.[2] One of them was VOC abatement, studied afterwards by other authors, such as van de Beld et al.[3], Eigenberger and Nieken,[4] and Sapundzhiev et al.[5] Complete reviews on the RFR technology are available in the bibliography.[6,7]

Correspondence concerning this article should be addressed to S. Ordóñez at sordonez@uniovi.es.

One of the most important problems found in the study of RFR is the difficulty for scaling-up these processes. The small-scale reactors present high surface-volume ratio, which leads to two main problems: it is not easy to get an adiabatic behavior, and the effect of the reactor walls in the reactor performance is more marked. A previous work of our research group provided a way, using an original temperature control system that nearly eliminates the heat losses through the wall, for overcoming this problem.[8]

Concerning the wall effects, it must be considered that the reactor wall is in thermal contact with both the catalytic bed and the fluid phase, and stores an amount of heat that can be relevant in the overall heat balance. On the other hand, the reactor wall conducts heat axially, affecting the temperature profiles and the heat wave creeping velocity with regard to those characteristic of the ideal (when such effect is not considered) or industrial (due to the low surface to volume ratio) case. The wall effects can then play an important role in systems like RFR, strongly based on the capability of retaining the high temperature zone of the axial profile within the limits of the bed.

In spite of the importance of the wall effects, very few bibliographic references use models that take into account the heat transfer phenomena involving the reactor wall in the energy balances, and, among these, only some of them study in some detail the resulting consequences in the reactor performance. Van de Beld et al.[3], used a reactor thermally isolated by an evacuated jacket presenting reduced heat loses, and a heterogeneous one-dimensional model taking into account the wall effect in the energy balances. They found that the wall effects cause an increase of the system overall heat dispersion, leading to a decrease of the temperatures and less steep temperature axial profiles.[9] For conditions not explicitly indicated, they also showed that the wall effects are more relevant when the switching time increases. They also studied the effect of the physical properties of the wall, concluding that heat capacity is the most important one, whereas thermal conductivity plays a minor role. Cittadini et al.[10] devoted part of their work on forced unsteady-state reactor development and design to point out that the key properties defining the extent of the wall effects are the thermal conductivity and wall thickness. They found that high wall thermal conductivities lead to heat bypass from the hot reactor center to the ends, making the system more prone to extinction and, therefore, diminishing the stability. This effect is more important as the wall thickness increases. Then, wall effects can be minimized by either diminishing the wall thickness or thermal conductivity. The first possibility is limited because the wall thickness cannot be reduced below a certain value. The second option could be effective, although it is difficult to find materials fulfilling the requirements of low thermal conductivity, high thermal resistance, and high mechanical resistance, needed for this application.

The aim of this study is to elucidate the intensity of the wall effects in small-scale RFR, and its dependence on the physical properties of the wall material. For this purpose, simulation and experimental results involving changes in both the thermal conductivity and the heat capacity of the wall were carried out. The range of these properties considered corresponds to the typical values of the materials used for this purpose. So, regarding thermal conductivity, Pyrex glass is the common material, with lower thermal conduction (1.2 $W{\cdot}m^{-1}{\cdot}K^{-1}$), less than half of that of quartz (3.0 $W{\cdot}m^{-1}{\cdot}K^{-1}$). Conductivity of stainless steel is 19.51 $W{\cdot}\ m^{-1}{\cdot}K^{-1}$, higher than that of common alloys such as Hastelloy, Inconel, and Monel (9.9, 10.0, and 17.0 $W{\cdot}\ m^{-1}{\cdot}K^{-1}$, respectively). Other metals have higher thermal conductivity, as copper and aluminum (381 and 283 $W{\cdot}\ m^{-1}{\cdot}K^{-1}$, respectively), but they are not widely suitable for building this kind of afterburners. Regarding $C_{pV,W}$, most common materials such as quartz (2.13 $J{\cdot}(m^3{\cdot}K)^{-1}$), Monel (3.77 $J{\cdot}(m^3{\cdot}K)^{-1}$), Inconel (3.57 $J{\cdot}(m^3{\cdot}K)^{-1}$), copper (3.23 $J{\cdot}(m^3{\cdot}K)^{-1}$) and aluminum (2.49 $J{\cdot}(m^3{\cdot}K)^{-1}$) are within the interval defined by Pyrex glass and stainless steel (1.86-3.85 $J{\cdot}(m^3{\cdot}K)^{-1}$).

The surface velocity of the gas in the afterburner largely affects the energy balances (convective heat transmission). So, the effect of this parameter on the wall effects must also be studied, resulting in an overall view of the reactor wall effects on the performance of RFR.

Methodology

Modeling and simulation

The dynamic behavior of the RFR was simulated using a heterogeneous one-dimensional model, defined by the PDE system formed by Eqs. 1-5. This set of equations is valid for modeling the catalytic combustion of methane. In our operation conditions, there is only one chemical reaction taking place (deep catalytic oxidation) and methane is the only reactant to be considered, since oxygen is a large excess. A more general model for a reverse flow reactor, considering more than one reaction and reactant, is described in our previous article.[8] Reaction of only one reactant (methane, in this case) and first order kinetics have been assumed. The first order kinetics simplification has been experimentally demonstrated to be accurate enough for this kind of catalysts, as indicated in the following section. Furthermore, and in good agreement with the literature findings,[11] mass accumulation in the catalyst surface was neglected and the validity of the steady-state approach of the continuity equation for the gas phase was assumed. Results reported in this work confirm that these assumptions do not lead to noticeable deviations in the temperature profiles prediction. The heat transmission between the bed and the reactor wall was considered to take place only through the gas phase (as in the aforementioned articles of Cittadini et al.[10] and van de Beld and Westerterp[9]). Further descriptions, including the model and the Fortran code used to solve it in the dynamic simulations, are available in Fissore et al.[8] and Hevia et al.[12] The main model parameters affecting the wall effects are wall thickness (d_w), heat capacity ($C_{p,W}$), density (ρ_W), conductivity (λ_W), and the gas feed surface velocity (u_0). Since $C_{p,W}$ and ρ_W always appear together in the model, it is more adequate to consider their product, the specific heat capacity, in a volumetric basis ($C_{p,W}\cdot\rho_W = C_{pV,W}$).

Gas phase energy balance:

$$\frac{\partial T_G}{\partial t} = -\nu\frac{\rho_{G,0}}{\rho_G}\frac{\partial T_G}{\partial x} + \frac{k_{eff}}{C_{p,G}\rho_G}\frac{\partial^2 T_G}{\partial x^2} + \frac{ha}{C_{p,G}\rho_G\varepsilon}(T_S - T_G) - \frac{4h_W}{C_{p,G}\rho_G D_R\varepsilon}(T_G - T_W) \quad (1)$$

Solid phase energy balance:

$$\frac{\partial T_S}{\partial t} = \frac{\lambda_{S,eff}}{C_{p,S}\rho_S}\frac{\partial^2 T_S}{\partial x^2} + \frac{(1-\varepsilon)\eta k_\infty(-\Delta H_c)\rho_G}{C_{p,S}\rho_S(1-\varepsilon)M}\exp(-E_a/RT_S)y_S - \frac{ha}{C_{p,S}\rho_G(1-\varepsilon)}(T_S - T_G) \quad (2)$$

Energy balance to the wall:

$$\frac{\partial T_W}{\partial t} = \frac{\lambda_W}{C_{p,W}\rho_W}\frac{\partial^2 T_W}{\partial x^2} + \frac{D_R h_W(T_G - T_W) - (D_R + 2d_W)h_{ext}(T_W - T_{ext})}{C_{p,W}\rho_W d_W(D_R + d_W)} \quad (3)$$

Gas phase mass balance:

$$\frac{\partial y_G}{\partial t} = -\nu\frac{\rho_{G,0}}{\rho_G}\frac{\partial y_G}{\partial x} + D_{eff}\frac{\partial^2 y_G}{\partial x^2} + \frac{K_G a}{\varepsilon}(y_S - y_G) \quad (4)$$

Solid phase mass balance:

$$K_G a(y_G - y_S) = (1-\varepsilon)\eta k_\infty \exp(-E_a/RT_S)y_S \quad (1^{st}\text{ order kinetics}) \quad (5)$$

$$K_G a(y_G - y_S) = 0 \quad \text{in the inert sections} \quad (6)$$

Experimental

Deep catalytic combustion of methane in lean air mixtures was studied in a novel bench-scale RFR unit. The reaction chamber consisted of a 0.8 m long and 0.05 m internal diameter cylinder, containing catalyst and inert material. The reactor gaseous feed (1000 ppmV methane in air) was made up by mixing air (from a compressor, filtered) and a mixture of 2.5%vol methane in synthetic air (from a gas cylinder). Mass flow regulators controlled the flow rate of both gases. A three-way valve, located downstream of the mixing point, allowed the feed to bypass the reactor for analytical purposes. The periodical flow reversals were accomplished by means of four solenoid valves. The main innovative feature of this reaction unit was a special temperature control system designed to dynamically compensate the heat losses through the wall, making it possible for the reactor to work very close to adiabatic conditions. A flow diagram of the apparatus is given in Figure 1, and a full description of this equipment, as well as the validation of its adiabatic performance can be found in a previous work.[8]

In previous experiments carried out in this device,[8,12] a metal oxides over alumina catalyst was used. In the present work, the catalyst was Pd (0.72wt%) on γ-Al_2O_3, in the form of 0.002-0.004 m diameter spheres, provided by BASF. This catalyst is less thermally stable than the metal oxides one, but more active, making it therefore possible to work at lower temperatures. This is important in this study, since one of the reactors used is made of Pyrex glass, material with limited working temperature (723 K for long periods). The reactor bed consisted of a central section of 0.240 m, containing the catalyst diluted with glass spheres, and two inert ending sections, 0.130 m each, containing 0.004 m diameter glass spheres.

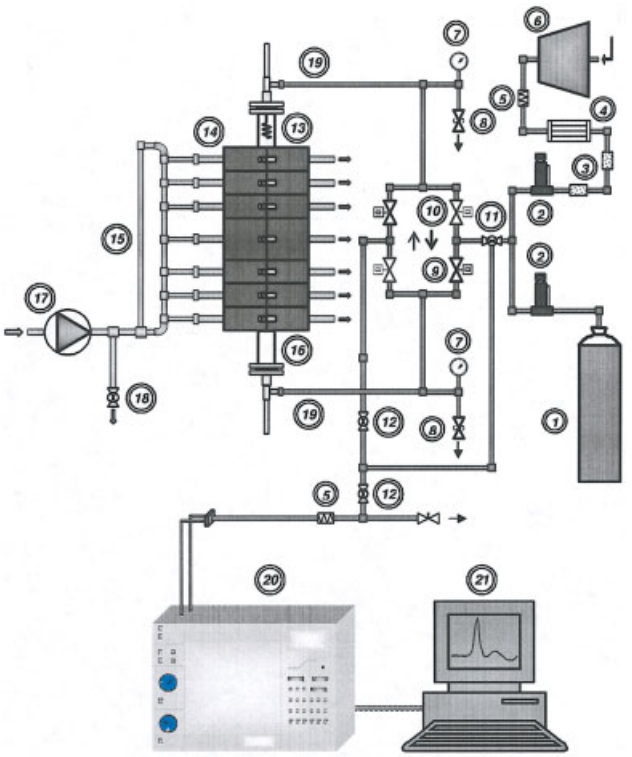

Figure 1. Experimental apparatus.

(1) Synthetic mixture air/CH_4. (2) Mass-flow controllers. (3) Oil filters. (4) Cooling dryer. (5) Particles filter. (6) Compressor. (7) Pressure gauges. (8) Relief valves. (9) Solenoid valves (downward flow when closed). (10) Solenoid valves (upward flow when closed). (11) Body valve (three-way). (12) Body valve (one way). (13) Preheater. (14) Modular oven. (15) Distribution of cooling air. (16) Reactor. (17) Blower. (18) Body valve (regulation). (19) Flexible tubing. (20) Gas chromatograph. (21) Computer. [Color figure can be viewed in the online issue, which is available at www.interscience.wiley.com.]

The intrinsic kinetics of the methane combustion on this catalyst was determined in an isothermal fixed bed microreactor described elsewhere.[13] In this study the catalyst was ground to $1\cdot10^{-4}$-$2.5\cdot10^{-4}$ m, ensuring that mass transfer resistances (internal and external) are negligible. The results fit well to a pseudo-first order expression with respect to methane,[14] as found in other works for the same reaction and type of catalyst.[15,16]

Two reactors made of different materials (Pyrex glass and stainless steel) were used in order to compare the effect of the reactor wall material on the reactor performance. The experimental conditions are summarized in Table 1, and selected in order to stress the different behavior of both materials, and to maintain the maximum reactor temperature below the aforementioned maximum allowable value for Pyrex glass.

Results and Discussion: Simulations

The reactor performance was studied by simulation through wide intervals of $C_{pV,W}$ (10^5-10^7 $J\cdot(m^3\cdot K)^{-1}$) and λ_W (1-25 $W\cdot m^{-1}\cdot K^{-1}$), maintaining constant the value for d_W (it should be taken into account that both the effects of $C_{pV,W}$ and λ_W are strengthened as d_W increases). The values of the properties for

Table 1. Main Operating Conditions and Physical Properties Used in This Work*

Properties of the Catalyst	
Pellet diameter (spheres), d_P	0.002-0.004 m
Density, ρ_S	1257 kg m^{-3}
Specific heat, $C_{p,S}$	836 J kg^{-1} K^{-1}
Inner porosity	0.519
Tortuosity	2
Thermal conductivity, λ_{eff}	0.042 W m^{-1} K^{-1}
Bed void fraction, ε	0.36
Pre-exponential factor, k_∞	$1.58 \cdot 10^{11}$ s^{-1}
Activation energy, E_a	$1.125 \cdot 10^5$ J mol^{-1}
Properties of the Bed Inert Material (glass)	
Diameter (spheres), $d_{P,i}$	0.004 m
Density, $\rho_{S,i}$	2590 kg m^{-3}
Specific heat	836 J kg^{-1} K^{-1}
Thermal conductivity, $\lambda_{eff,i}$	0.65 W m^{-1} K^{-1}
Inert endings volumetric fraction	0.52
Operating Conditions	
Surface velocity, u_0	0.108 m s^{-1} (calculated at $T_{G,0}$)
Preheating temperature, $T_{S,0}$	624-633 K
Inlet gas temperature, $T_{G,0}$	298 K
Inlet concentration, $y_{G,0} \cdot 10^6/\Delta T_{ad}$	1000/26.8 K
WHSV	2.26-2.36 h^{-1}
t_c	300 s
Pyrex Glass Reactor	
Volumetric specific heat, $C_{pV,W}$	$1.86 \cdot 10^6$ J $(K\ m^3)^{-1}$
Thermal conductivity, λ_W	1.2 W m^{-1} K^{-1}
Wall thickness, d_W	$2.89 \cdot 10^{-3}$ m
Stainless Steel Reactor	
Volumetric specific heat, $C_{pV,W}$	$3.85 \cdot 10^6$ J $(K\ m^3)^{-1}$
Thermal conductivity, λ_W	19.51 W m^{-1} K^{-1}
Wall thickness, d_W	$1.15 \cdot 10^{-3}$ m

*When some value differs from those appearing in this table, it is indicated in the figure captions.

the common building materials for fixed bed catalytic reactors are included in the studied intervals.

Results indicate that variations of $C_{pV,W}$ and λ_W lead to very important differences in the reactor temperature profiles, as shown in Figures 2 and 3. An increase of both variables leads to a decrease of the maximum temperature in the reactor. This behavior is much more marked for the wall thermal conductivity, the plateau in the temperature profile almost disappearing for the highest value of this property considered (25 $W \cdot m^{-1} \cdot K^{-1}$). As λ_W decreases, the temperature profiles gradually approximate to those corresponding to an absence of wall effects, wall effects being negligible for conductivities lower than 0.1 $W \cdot m^{-1} \cdot K^{-1}$. The effect of $C_{pV,W}$ is similar, but less marked, and at the conditions studied ($\lambda_W = 1$ $W \cdot m^{-1} \cdot K^{-1}$ (Figure 3, curves b-e)), the temperature profiles are not affected for values of $C_{pV,W}$ below 10^6 $J \cdot (m^3 \cdot K)^{-1}$. The effect of $C_{pV,W}$ on the temperature profiles is even less marked when the value of λ_W is higher, as can be seen in Figure 3, curves f-h.

The range of stable operation is as important as temperature profiles in the operation of RFR. The RFR stability can be discussed in terms of the critical switching time ($t_{c,\ crit}$), that is, the maximum switching time that allows obtaining an ignited PSS. Figure 4 illustrates the effect of the wall heat capacity and thermal conductivity on the RFR stability, and the interactions between both parameters. The results confirm that the influence

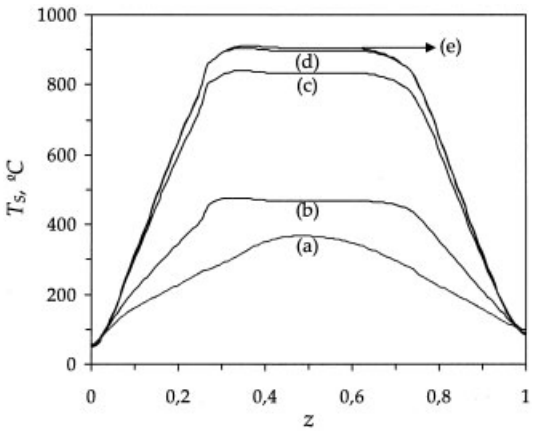

Figure 2. Influence of the wall thermal conductivity: temperature profiles at the middle of a semi-cycle at the PSS (t_c = 600 s, $d_W = 10^{-3}$ m, $C_{pV,W} = 10^6$ $J \cdot (m^3 \cdot K)^{-1}$).

Curve (a): $\lambda_W = 25$ $W \cdot (m \cdot K)^{-1}$; curve (b): $\lambda_W = 10$ $W \cdot (m \cdot K)^{-1}$; curve (c): $\lambda_W = 1$ $W \cdot (m \cdot K)^{-1}$; curve (d): $\lambda_W = 0.1$ $W \cdot (m \cdot K)^{-1}$; curve (e): *No wall effects*.

of λ_W is most important, the stability always diminishing as λ_W increases. The effect of the heat conductivity is more marked at higher values of the heat capacity.

The effect of $C_{pV,W}$ is less pronounced, and depends on the value of λ_W. Thus, for low thermal conductivities, an increase of the heat capacity leads to an increase in $t_{c,\ crit,}$ while for high conductivities the effect is just the opposite. At intermediate conductivity values, the evolution of $t_{c,\ crit}$ with $C_{pV,W}$ presents a maximum.

It is remarkable that, while for the case of no wall effects, the value calculated for $t_{c,\ crit}$ is 3115 s, yet results in Figure 4 show a region (corresponding to low conductivities and high heat capacities) for which $t_{c,\ crit}$ are higher, indicating that in such

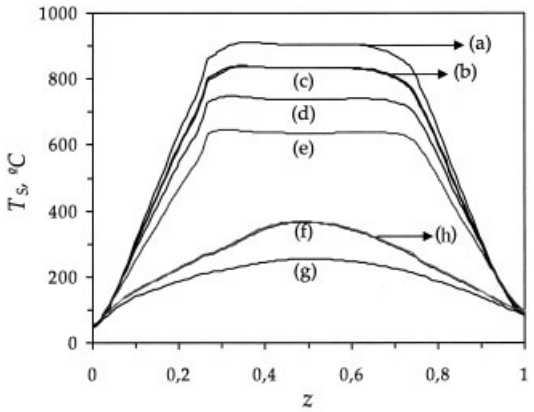

Figure 3. Influence of the wall heat capacity: temperature profiles at the middle of a semi-cycle at the PSS; Z represents the dimensionless reactor length (t_c = 600 s, $d_W = 10^{-3}$ m).

(a): *No wall effects*. Curves (b)-(e): $\lambda_W = 1$ $W \cdot (m \cdot K)^{-1}$; (b): $C_{pV,W} = 10^5$ $J \cdot (m^3 \cdot K)^{-1}$; (c): $C_{pV,W} = 10^6$ $J \cdot (m^3 \cdot K)^{-1}$; curve (d): $C_{pV,W} = 5 \cdot 10^6$ $J \cdot (m^3 \cdot K)^{-1}$, (e): $C_{pV,W} = 10^7$ $J \cdot (m^3 \cdot K)^{-1}$. Curves (f)-(h): $\lambda_W = 25$ $W \cdot (m \cdot K)^{-1}$; (f): $C_{pV,W} = 10^5$ $J \cdot (m^3 \cdot K)^{-1}$; (g): $C_{pV,W} = 10^6$ $J \cdot (m^3 \cdot K)^{-1}$; (h) $C_{pV,W} = 5 \cdot 10^6$ $J \cdot (m^3 \cdot K)^{-1}$.

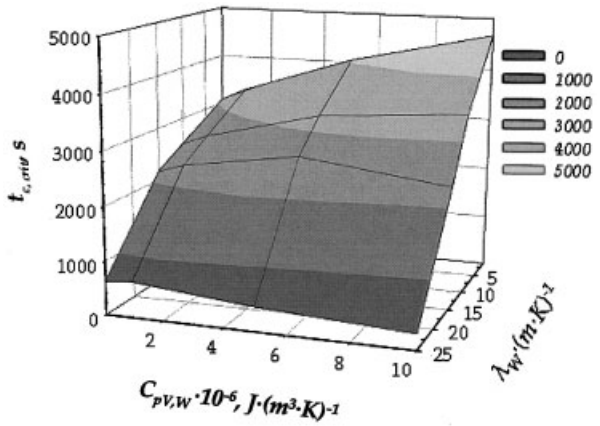

Figure 4. Stability surface depending on $C_{pV,W}$ and λ_W ($d_W = 10^{-3}$ m).

conditions the wall effects produce an improvement in the RFR stability.

This behavior can be explained by a two-fold effect of the wall heat capacity on the reactor stability:

- *Negative:* The higher $C_{pV,W}$, the higher the amount of heat necessary to increase/decrease the wall temperature, and hence, the higher the ratio of the total heat produced in the system that circulates through the wall. This results in a decrease of the temperature in the bed catalytic section, as shown in Figures 2 and 3.
- *Positive:* High values of $C_{pV,W}$ contribute to slow down the movement of the bed high temperature wave, leading to an increase of the stability.

The negative effect of $C_{pV,W}$ prevails for high wall conductivities, whereas the positive one is dominant for low wall conductivities.

The nature of the wall effects on the RFR stability depends, then, on the ratio between the creeping velocity of the high temperature wave in the bed and in the wall. According to this, gas surface velocity would affect strongly the nature of the wall effects, as surface velocity influences markedly the creeping velocity of the temperature wave in the bed, but has no direct effect on the wall. Then, we can expect that the relevance of the wall effects in the system would decrease as the surface velocity increases, and hence, the stability of the reactor would approach that of the system with no wall effects. Results shown in Figure 5, where reactor temperature profiles for different surface velocities are presented, show this behavior. Figure 6, where $\Delta t_{c,\,crit}$ (the difference between $t_{c,\,crit}$ calculated with and without wall effects) is represented as a function of wall conductivity and gas surface velocity, confirms this trend. So, it is observed that even in the worst cases (the highest values of λ_w), the negative wall effects can be suppressed by working at high enough surface velocities. On the other hand, working with low heat conductivity materials allows the reactor to operate in a wide range of surface velocities (and, hence, residence times) with negligible wall effects.

Therefore, it can be concluded that the relevance of wall effects decreases for low conductivity building materials for the reactor (as expected), and for high gas surface velocities.

Results and Discussion: Experimental Essays

In previous studies[8,12,14] the mathematical model used here was proved to accurately predict the behavior of our experimental unit fitted with a stainless steel reactor. The following step is to check experimentally the sensitivity of the behavior of the reactor to the physical properties of the wall, and to compare the experimental results with model predictions for other reactor materials, in order to validate experimentally the conclusions drawn from simulations. For this purpose, the experimental unit was operated with two reactors, identical in dimensions, constructed in stainless steel and Pyrex glass, representing materials with high and low thermal conductivity, respectively. The operating conditions for the experiment were fixed taking into account two main requirements: the expected performances should be different enough to be clearly observed, and working temperatures should not reach the maximum allowable temperature for Pyrex glass, that is, 723 K. Furthermore, the number of experiments that could be carried

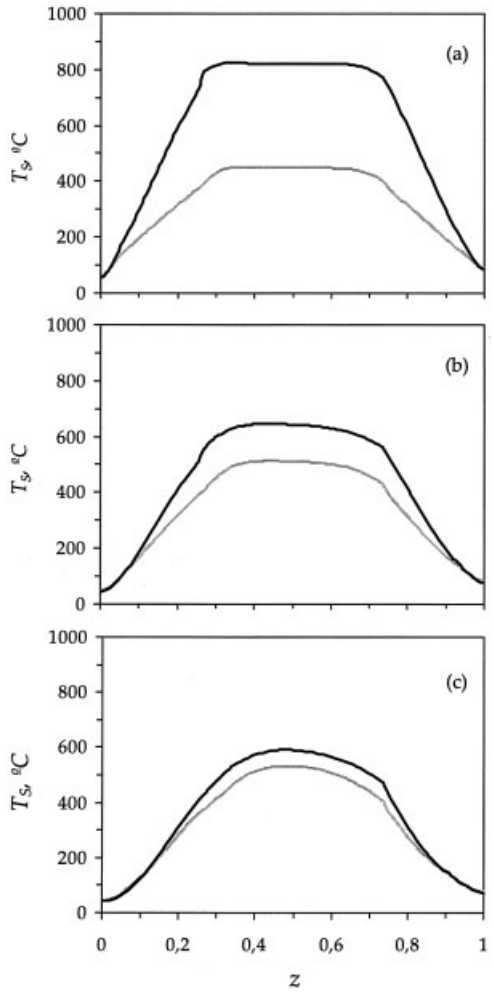

Figure 5. Influence of the gas surface velocity on the wall effects: temperature profiles at the middle of a semi-cycle at the PSS (t_c = 200 s, $d_W = 10^{-3}$ m, λ_W = 25 W·(m·K)$^{-1}$); $C_{pV,W} = 10^6$ J·(m^3·K)$^{-1}$).

(—) *With wall effects*; (—) *Without wall effects*. (a): u_o = 0.25 m/s; (b): u_o = 0.50 m/s; (c): u_o = 0.75 m/s.

out was limited, due to the tendency of breaking of the Pyrex glass reactors, caused by the mechanical tensions produced in the flanges and with the oven. The most important operating conditions for the experiments are indicated in Table 1 and the caption of Figure 7. According to model predictions, at the selected operating conditions, the stainless steel reactor should go towards extinction after $1.8\ 10^4$ s, while the Pyrex unit should continue in stable operation.

The experimental results obtained are depicted in Figure 7 in terms of the bed center temperature evolution with time, for both wall materials. In both cases, the simulated results are also plotted. The remarkably different results obtained for both wall materials confirm the relevance of the reactor wall physical properties on the performance of lab-bench scale RFR. The steel reactor tends to extinction and the Pyrex one maintains stable operation, as anticipated by the model. It can also be observed that the experimental and simulated values are very close to each other through the experiment.

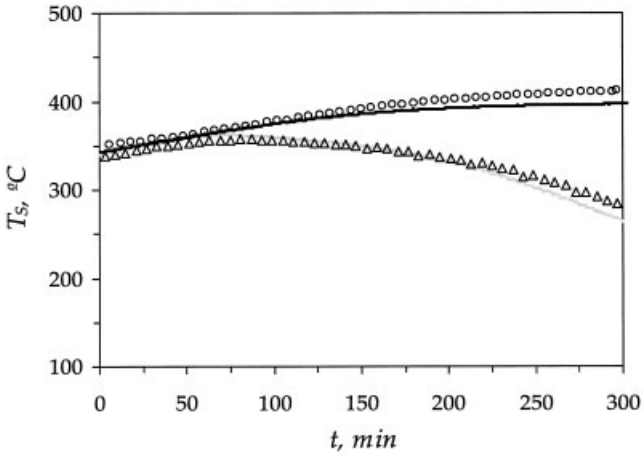

Figure 7. Simulated (—steel, —Pyrex) and experimental (Δ steel, o Pyrex) evolution of the temperature at the reactor center ($y_{G,O}\cdot 10^6 = 1000$).

Conclusions

In this work, the relevance of wall effects on the performance of small and medium-sized RFR units has been demonstrated, both from modeling studies and experimentally. Wall effects can largely change the reactor temperature profile and dramatically diminish the range of stable operation. Since the extent of the wall effects increases as the surface to volume ratio increases, wall effects are a gap to be taken into account when scaling-up results from small units to larger reactors. The physical properties of the reactor wall building material determine the extent of these effects. Specifically, as the thermal conductivity and the heat capacity increase, the bed temperature decreases. With regard to the stability range, it always decreases as the thermal conductivity increases. The influence of the heat capacity in the stability is more complex since it depends on the range of thermal conductivities considered. On the other hand, the relevance of wall effects depends also on the gas surface velocity, decreasing as the surface velocity increases.

According to the results of this work, two guidelines can be adopted for minimizing the impact of wall effects in the performance of RFR units. First, low thermal conductivity materials, such as ceramics, quartz, or Pyrex glass, are more appropriate for the construction of lab-bench RFR. Unfortunately, these materials are fragile and tend to break. Second, the higher the surface gas velocity, the lower the importance of wall effects.

The simulation results were in good agreement with the results of experiments performed with reactors constructed in Pyrex glass and a stainless steel. Therefore, although wall effects in lab-bench scale RFR cannot be avoided, mathematical dynamic models taking into account wall effects can predict fairly well such effects, being then a powerful tool for the design of RFR reactors, as well as for the scale-up and the interpretation of the results obtained.

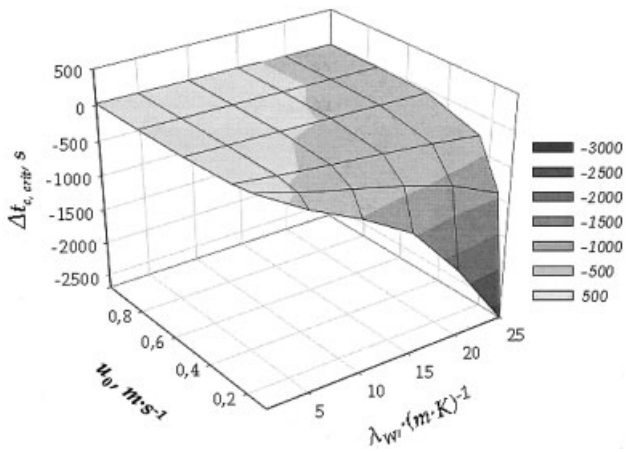

Figure 6. Influence of wall effects on RFR stability: $\Delta t_{c,\,crit}$ as a function of u and λ_W ($d_W = 10^{-3}$ m, $C_{pV,W} = 10^6$ J·(m^3·K)$^{-1}$)).

Acknowledgments

This work has been financially supported by the European Commission (Contract ENV4-CT97–0599) and the Government of the Principality of Asturias through the research project ref. FC-03-PB02–133. Profs. Giancarlo Baldi, Antonello Barresi, and Marco Vanni (*Politecnico di Torino*) are also gratefully acknowledged for their contributions in the modeling of the system and in the design of the experimental unit. The catalyst used for these experiments was a generous gift of BASF.

Notation

a = external particle surface area per unit volume of reactor, m^{-1}
C_p = specific heat at constant pressure, J kg^{-1}K^{-1}
D_{eff} = effective mass dispersion coefficient, m^2 s^{-1}
d_P = pellet diameter, m
D_R = reactor inner diameter, m
d_W = wall thickness, m
E_a = activation energy, J kmol^{-1}
h = gas-solid heat transfer coefficient, J m^{-2}K^{-1}s^{-1}
k_∞ = pre-exponential factor, s^{-1}
k_{eff} = effective heat dispersion coefficient, J m^{-1}K^{-1}s^{-1}
K_G = gas-solid mass transfer coefficient, m s^{-1}
M = molecular weight of the gas mixture, g mol^{-1}
R = ideal gas constant, J K^{-1} mol^{-1}
T = temperature, K
t = time, s
t_c = switching time, s
u = surface velocity, m s^{-1}
v = interstitial velocity, m s^{-1}

x = axial reactor coordinate, m
y = molar fraction
ΔH_c = enthalpy of combustion, J mol^{-1}
$\Delta t_{c,\,crit} = (t_{c,\,crit})_{\text{with wall effects}} - (t_{c,\,crit})_{\text{without wall effects}}$

Greek letters

ΔT_{ad} = adiabatic temperature increase, K
ε = bed void fraction
λ = thermal conductivity, J m^{-1} K^{-1} s^{-1}
ρ = density (or apparent density for the catalyst), kg m^{-3}
η = intraparticle effectiveness factor

Subscripts and superscripts

ext = inlet conditions
crit = critical value
ext = external property
G = gas phase
i = inert material
S = solid phase or solid surface
V = volumetric base
W = reactor wall

Abbreviations

PDE = Partial Derivative Equation system
RFR = Reverse-Flow Reactor
PSS = Periodic Steady State

Literature Cited

1. Boreskov GK, Matros YS. Unsteady-state performance of heterogeneous catalytic reactors. *Catal Rev - Sci Eng.* 1983;25:551-590.
2. Matros YS. *Catalytic Processes Under Unsteady-State Conditions*. Amsterdam, Netherlands: Elsevier Science Publishers B.V.; 1989.
3. van de Beld B, Borman RA, Deckx OR, van Woezik BAA, Westerterp KR. Removal of volatile organic compounds from polluted air in a reverse flow reactor: an experimental study. *Ind Eng Chem Res.* 1994;33:2946-2956.
4. Eigenberger G, Nieken U. Catalytic combustion with periodic flow reversal. *Chem Eng Sci.* 1988;43:2109-2115.
5. Sapundzhiev C, Grozev G, Elenkov D. Non steady-state catalytic decontamination of waste gases. *Chem Eng Technol.* 1991;14:209-212.
6. Matros YS, Bunimovich GA. Reverse-flow operation in catalytic reactors. *Catal Rev - Sci Eng.* 1996;38:1-68.
7. Hevia MAG, Ordóñez S, Díez FV. Catalytic reactors with periodic flow reversal: operation, modelling and applications. *Afinidad.* 2003; 60:422-428.
8. Fissore D, Barresi A, Baldi G, Hevia MAG, Ordóñez S, Díez FV. Design and testing of small-scale unsteady-state afterburners and reactors. *AIChE J.* 2005;51:1654-1664.
9. van de Beld L, Westerterp KR. Air purification in a reverse-flow reactor: model simulations vs. experiments. *AIChE J.* 1996;42:1139-1148.
10. Cittadini M, Vanni M, Barresi A, Baldi G. Development and design of a forced unsteady-state reactor through numerical simulation. *Computer Aided Chemical Engineering 8*. Pierucci S (ed.). Amsterdam: Elsevier Science Publishers B.V.; 2000:697-702.
11. Fissore D, Barresi AA. Comparison between the reverse-flow reactor and a network of reactors for the oxidation of lean VOC mixtures. *Chem Eng Technol.* 2002;25:421-426.
12. Hevia MAG, Ordóñez S, Díez FV, Fissore D, Barresi A. Design and testing of a control system for reverse-flow catalytic afterburners. *AIChE J.* 2005;51:3020-3027.
13. Hurtado P, Ordóñez S, Díez FV, Sastre H. Development of a kinetic model for the oxidation of methane over Pd/Al_2O_3 at dry and wet conditions. *Appl Catal, B.* 2004;51:229-238.
14. Hevia MAG. Catalytic combustion of methane in reverse flow reactors: design, operation and simulation. Ph.D. Thesis, Universidad de Oviedo, Spain, 2004.
15. Lee JH, Trimm DL. Catalytic combustion of methane. *Fuel Process Tech.* 1995;42:339-359.
16. Lyubovsky M, Pfefferle L. Complete methane oxidation over Pd catalyst supported on γ-alumina. Influence of temperature and oxygen pressure on the catalyst activity. *Catal Today.* 1999;47:29-44.

Manuscript received Jan. 30, 2006, and revision received May 9, 2006.